Interaction of CH_4, CH_3Cl, CH_2Cl_2, $CHCl_3$, and CCl_4 with O-Terminated FeO(111)

Shu-Rong Liu, Z. Dohnálek,* R. Scott Smith, and Bruce D. Kay*

Fundamental Sciences Directorate, Pacific Northwest National Laboratory, P.O. Box 999, MSN K8-88, Richland, Washington 99352

Received: November 10, 2003; In Final Form: January 16, 2004

Well-ordered FeO(111) thin films are epitaxially grown on a Pt(111) substrate. A series of molecules including CH_4, CH_3Cl, CH_2Cl_2, $CHCl_3$, and CCl_4 are used as probes to test the chemical reactivity of the FeO(111) surface. The temperature-programmed desorption spectra show no evidence of dissociative adsorption or chemical reaction between the substrate and the adsorbates. The desorption kinetics studies reveal that all the molecules are physisorbed and have desorption kinetics with an order between 0 and 1. Kinetic analysis is conducted, assuming both zero- and first-order desorption, and shows that an uncertainty in the desorption order introduces an error in determination of the terrace site desorption energies ($\theta = 0.5$ ML) of only ~2%. The desorption energies for the series of molecules increase with the number of chlorine atoms in the molecule. The increase of desorption energies is not linear with the molecular polarizability, and the deviations from linearity are attributed to the permanent dipole in some of the molecules. We conclude that the oxygen-terminated FeO(111) surface is in general unreactive toward both C−H and C−Cl bonds in methane and its chlorinated derivatives.

I. Introduction

Metal oxides constitute an important class of materials and are used in a wide range of catalytic and environmental science applications. A large number of organic compounds are industrially synthesized on oxide catalysts using various reaction schemes such as selective oxidation, dehydrogenation, and isomerization. In environmental applications, oxides are primarily used to alter or immobilize environmentally harmful pollutants.[1] The optimization of the activity of an oxide for a particular chemical application requires an understanding of the factors that control its reactivity. The role the oxidation state of the metal, coordination of the metal at a particular surface site, and the surface orientation play in the reactivity of the oxide is very often unknown. Studies performed under controlled experimental conditions on various surfaces and phases of a given oxide are essential to unravel the factors that determine particular structure−reactivity relationships.

There are a number of iron oxides with different stoichiometries, phases, and crystal structures and as such represent an ideal platform for studying such structure−reactivity relationship.[1] The iron oxides include FeO (wüstite), Fe_3O_4 (magnetite), α-Fe_2O_3 (hematite), γ-Fe_2O_3 (maghemite), and ϵ-Fe_2O_3. The first three phases occur naturally, but the latter two phases have only been synthesized under controlled conditions in the laboratory. At thermodynamic equilibrium, the stability range of the individual phases depends on the ambient O_2 pressure and the temperature.[1]

Reproducible preparation of high-purity, monocrystalline iron oxide samples of known composition and phase is the first step in the study of their distinctive reactivities. Samples obtained from bulk metal oxides often contain impurities that can segregate to the surface upon annealing under ultrahigh vacuum conditions. Sputtering, often used on metals to remove such impurities, can lead to irreversible damage on oxide surfaces.[1−3] The oxidation of pure iron single-crystal surfaces is also questionable since it is difficult to produce monocrystalline films with controlled composition and thickness.[1,2] An alternate approach is to grow epitaxial thin films of the oxide on dissimilar metal substrates with a good lattice match of the desired oxide composition and orientation. There are several excellent general reviews regarding the growth of thin oxide films on metal substrates.[4−8] This has been shown to be a powerful method in the preparation of model oxide surfaces with controlled orientation and defect density necessary to yield a better understanding of surface reactivity.[1−3]

High-quality thin films of FeO(111), Fe_3O_4(111), and α-Fe_2O_3-(0001) have been epitaxially grown on a Pt(111) substrate and studied in detail by various experimental methods and theoretical calculations.[1−3,9−11] Techniques such as scanning tunneling microscopy (STM),[12,13] high-resolution transmission electron microscopy (HRTEM),[14] high-resolution low-energy electron diffraction (LEED),[13,15] and X-ray photoelectron diffraction (XPD) have been employed to determine their surface structure.[16] More recently, investigations have focused on the metal-oxide interface[17] and the reactivity of these films.[18−25] Studies of water and ethylbenzene adsorption on FeO(111) and Fe_3O_4-(111) surfaces have shown that the reactivity is strongly correlated with the presence of surface iron.[18−21] For example, the Fe-terminated Fe_3O_4(111) surface dissociates H_2O, whereas the O-terminated FeO(111) does not.[18,19]

The reactivity of carbon tetrachloride on various iron oxide surfaces was explored previously in several studies.[23,24,26−29] The Fe-terminated Fe_3O_4(111)[23,24,26] and Fe(110)[27−29] surfaces were shown to facilitate the dissociation of CCl_4. No studies were reported on FeO(111) thin films. In contrast with other iron oxide surfaces, the thin FeO(111) films deposited on Pt-(111) form polar, unreconstructed surfaces terminated by a close-packed layer of oxygen,[1] as shown in Figure 1a. Since this surface does not have any surface iron, it represents a good

* Authors to whom correspondence should be addressed. E-mail: Zdenek.Dohnalek@pnl.gov; Bruce.Kay@pnl.gov.

10.1021/jp0312363 CCC: $27.50
Published on Web 02/20/2004

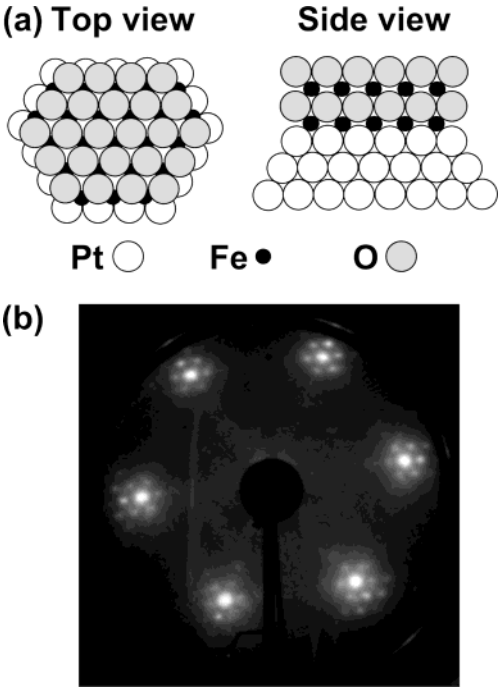

Figure 1. (a) A schematic of the FeO(111) thin film surface grown on a Pt(111) substrate. The top layer is oxygen terminated. (b) The LEED pattern from a 2 ML thick FeO(111) surface for an electron energy of 63 eV.

reference for comparison with the reactivity of Fe-terminated iron oxide surfaces.

In this study, we investigate the adsorption/desorption kinetics of methane, CH_4, and its chlorinated derivatives, CH_3Cl, CH_2Cl_2, $CHCl_3$, and CCl_4, on two-monolayer-thick O-terminated FeO(111) thin films deposited on Pt(111). High-quality temperature-programmed desorption (TPD) measurements show that all studied species adsorb and desorb molecularly. An inversion analysis of the temperature-programmed desorption spectra is used to extract the desorption kinetic parameters.[30] The desorption energies for the series generally increase with increasing polarizability; however, the presence of a dipole moment in some of the molecules causes a small deviation from a linearity. In the adsorption experiments, all the chlorinated molecules have initial sticking probabilities on clean FeO(111) that approach unity, whereas methane exhibits a lower initial sticking probability of ~0.6.

II. Experimental Section

The experiments were conducted in an ultrahigh vacuum (UHV) chamber with a base pressure of $\sim 1 \times 10^{-10}$ Torr. The Pt(111) substrate was cleaned using standard procedures including a sequence of neon-ion bombardment, O_2 annealing at 1200 K (5 min, 2×10^{-7} Torr), and annealing in UHV at 1300 K. The temperature of the Pt(111) substrate was measured using a chromel−alumel (type K) thermocouple spot welded to the edge of the sample and could be controlled from 20 to 1300 K. An absolute temperature calibration was performed using the multilayer desorption of various gases (N_2, Ar, O_2, and H_2O) from the sample surface.[31] The resulting uncertainty in the absolute temperature is estimated to be ±2 K. The surface purity and order of the Pt(111) and FeO(111) surfaces were checked using Auger electron spectroscopy (AES) and low-energy electron diffraction (LEED).

Thin FeO(111) films (~2 ML thick) were grown epitaxially on the Pt(111) substrate using a previously published procedure.[1,9] The iron was evaporated onto the Pt(111) substrate using a high-temperature effusion-cell (CreaTec). The deposition flux of Fe was measured using a Quartz-Crystal microbalance (QCM XTM/2-Inficon) deposition monitor and was found to be stable on a day-to-day basis. An iron deposition rate of ~2 ML/min was used in this study. To grow a film, one monolayer of Fe was deposited on the Pt(111) surface at 300 K, and then oxidized at 870 K in an O_2 atmosphere (3 min, 10^{-6} Torr). An additional cycle of Fe deposition and O_2 oxidation at 1000 K (3 min, 1×10^{-6} Torr) was employed to obtain the final 2 ML thick FeO(111) film. This process proved to be highly reproducible and yielded high quality FeO(111) films.

The adsorbates that are liquids at room temperature, CH_2Cl_2 (Aldrich, 99.9%, A.C.S. HPLC grade), $CHCl_3$ (Sigma-Aldrich, 99.9+%, A.C.S. HPLC grade), and CCl_4 (Aldrich, 99.9+%, HPLC grade), were purified by two or three freeze−pump−thaw cycles to remove the more volatile contaminants before dosing. The gaseous adsorbates CH_4 (Air Liquide, 99.99%) and CH_3Cl (Specialty Products & Equipment, 99.9%) were dosed as received. All molecules were introduced using a neat, 300 K, quasi-effusive molecular beam[30] directed normal to the FeO(111) surface at 22 K. The sticking coefficients were measured using the beam reflection technique of King and Wells.[31,32] All TPD spectra were acquired using a line-of-sight quadrupole mass spectrometer and a linear temperature ramp rate of 1 K/s.

III. Results and Discussion

A. Characterization of FeO(111) Films by LEED and N_2 Physisorption. Figure 1b shows a typical LEED image from a 2 ML thick film FeO(111). The corresponding structure was determined previously[1] and is shown in Figure 1a. The LEED pattern consists of six main bright diffraction spots, which come from the hexagonal Fe−O bilayer with O-termination. Each of the six main spots is surrounded by smaller satellite spots coming from the Pt substrate diffraction and multi-diffraction between the Pt substrate and the FeO due to the lattice mismatch.[1] This LEED image shows that our FeO(111) films are highly ordered and have quality comparable to those obtained in previous studies.[1]

To further check the quality of the FeO(111) surface we determined the distribution of surface binding sites using the desorption of an N_2 monolayer. In our previous studies, we have shown that the desorption energies of weakly bound species on oxides (e.g., N_2 or CO on MgO (100)) are strongly affected by the type of adsorption sites.[30,33] This is in agreement with theoretical calculations that show that the surface sites with lower coordination (e.g., steps, kinks, or vacancies) lead to increased binding energies of physisorbed adsorbates.[34]

A set of N_2 TPD spectra obtained from the (111) surface of a 2 ML thick FeO film as a function of initial N_2 coverage ranging from 0.11 ML to 1.57 ML is shown in Figure 2. For coverages below 0.11 ML, N_2 desorption at high temperature (>50 K) is observed and is assigned to the desorption from defect sites or defect-influenced sites.[30,33] For increasing N_2 coverages in the 0.17−0.86 ML range, a first-order desorption feature from FeO(111) terrace sites appears and saturates. At higher coverages, the multilayer desorption peak appears between 30 and 35 K. The minimum defect coverage that we have been able to achieve is ~0.11 ML. The low percentage of defects indicates that the film is highly ordered and is comparable in quality to a single crystal.

B. Sticking Coefficient Measurements. Figure 3 displays the sticking coefficients for CH_4, CH_3Cl, CH_2Cl_2, $CHCl_3$, and CCl_4 on FeO(111) plotted versus their relative coverage on the

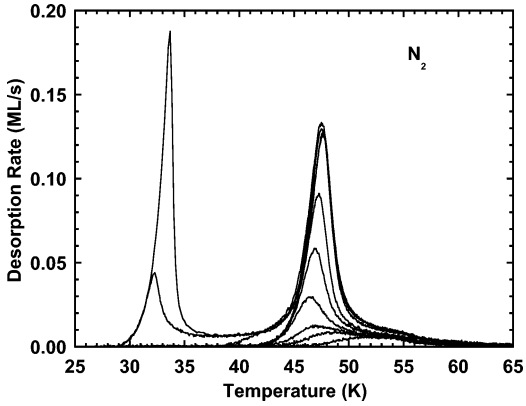

Figure 2. The TPD spectra of submonolayer, monolayer, and multilayer N_2 from FeO(111) for a variety of initial coverages (θ = 0.11, 0.17, 0.20, 0.33, 0.48, 0.60, 0.86, 1.00, 1.14, and 1.57 ML). The ramp rate here was 0.6 K/s.

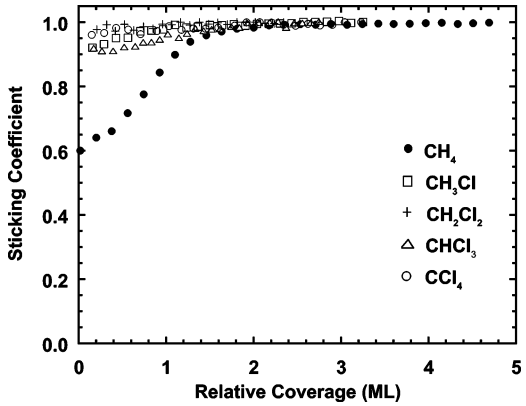

Figure 3. The sticking coefficients of CH_4, CH_3Cl, CH_2Cl_2, $CHCl_3$, and CCl_4 molecules on FeO(111) as a function of adsorbate coverage. The substrate temperature was held at 22 K during the sticking measurement in all experiments.

surface. The sticking coefficients were determined using the beam reflection technique of King and Wells,[32] and the detailed description of the procedure used to extract their coverage dependence was described previously.[30] The mean kinetic energy of the 300 K quasi-effusive beam was ~5 kJ/mol. The data in Figure 3 show that the initial sticking coefficient, S_0, on clean FeO(111) is large ($S_0 > 0.9$) for all chlorinated molecules and approaches unity on monolayer-covered FeO(111). The values of S_0 are 0.92 ± 0.05 for CH_3Cl and $CHCl_3$; the values are 0.97 ± 0.05 for CH_2Cl_2 and CCl_4. The high initial sticking coefficient is a result of efficient energy transfer between the adsorbates and the surface.

In contrast with the high S_0 observed for Cl-containing molecules, S_0 for CH_4 is significantly lower, 0.60 ± 0.05. On the basis of simple kinematic arguments, one would expect a high value for S_0 since the mass of CH_4 is the same as the surface O atoms. Therefore, the lower than unity sticking is most likely the consequence of FeO lattice stiffness. The sticking coefficient for CH_4 increases linearly with increasing adsorbate coverage analogous with the CH_4 sticking on MgO(100) that was reported previously.[30] Such a linear increase in the sticking coefficient can be understood by assuming constant but different CH_4 sticking coefficients on clean (S_0) and CH_4-covered (S_1) FeO(111). The coverage-dependent sticking coefficient, $S(\theta)$, can be described as a linear combination of the S_0 and S_1 weighted by relative surface areas of clean and CH_4-covered surface, $S(\theta) = S_0(1 - \theta) + S_1\theta$. For the second CH_4 layer, the sticking coefficient increases approximately linearly from 0.85 to 1.0 as the coverage increases from 1 to 2 ML. Therefore, the mechanism of the sticking in the second layer is likely analogous to that of the first layer. Beyond ~2 ML, the sticking coefficient approaches unity (within experimental uncertainty) and remains constant for CH_4 condensation on CH_4 multilayers. The fact that the sticking coefficient on a complete CH_4 monolayer has not reached unity is most probably caused by imperfect energy transfer on the FeO-bound CH_4 monolayer.

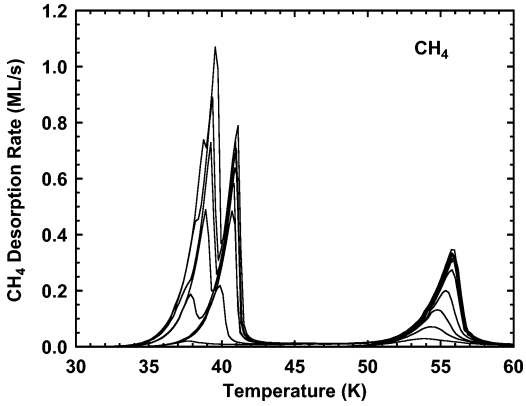

Figure 4. The TPD spectra of submonolayer, monolayer, and multilayer CH_4 from FeO(111) for a variety of initial coverages (θ = 0.16, 0.34, 0.42, 0.60, 0.75, 1.00, 1.11, 1.34, 1.80, 2.16, 2.65, 3.34, 3.99, and 4.18 ML). The ramp rate here and in subsequent TPD experiments was 1 K/s.

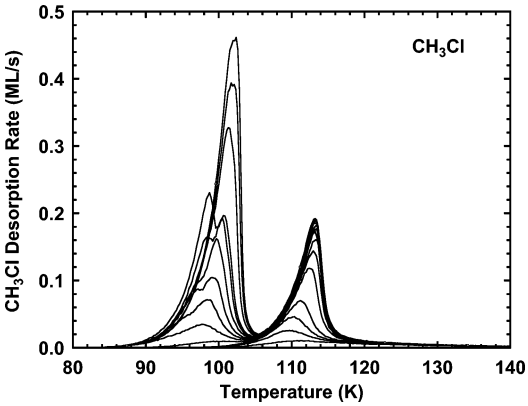

Figure 5. The TPD spectra of submonolayer, monolayer, and multilayer CH_3Cl from FeO(111) for a variety of initial coverages (θ = 0.23, 0.34, 0.44, 0.54, 0.77, 0.88, 1.00, 1.25, 1.47, 1.70, 1.92, 2.18, 2.45, 2.63, 2.89, and 4.18 ML).

C. Temperature-Programmed Desorption. Coverage-dependent TPD spectra for CH_4, CH_3Cl, CH_2Cl_2, $CHCl_3$, and CCl_4 on the FeO(111) surface are shown in Figures 4-8, respectively. The relative coverages are obtained by normalizing the area under the desorption spectra relative to the area under the spectrum with saturated adsorption sites in the first layer (one monolayer) and no adsorption in the second layer.

Figure 4 shows the TPD spectra of CH_4 from the FeO(111) surface for initial coverages ranging from 0.16 to 4.18 ML. The spectra for initial coverages less than or equal to 1 ML exhibit a single desorption feature peaked between 54 and 57 K. The desorption curves exhibit common leading edges for all exposures as expected for coverage-independent zero-order desorption kinetics. However, the desorption rate does not decrease sharply from the maximum to zero, but instead decreases gradually as expected for first-order desorption. Thus, these TPD spectra show characteristics suggestive of both zero- and first-order desorption kinetics. The second and third layers desorb with zero-order kinetics from 37 to 42 K and from 33

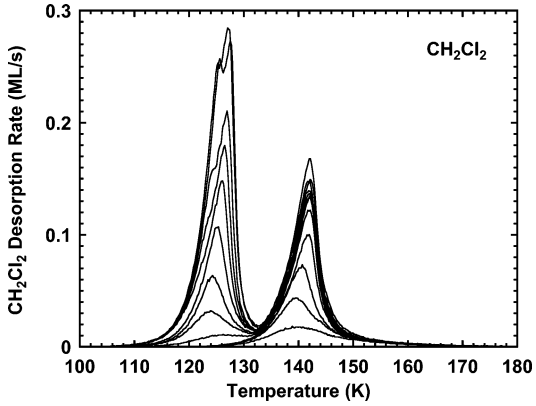

Figure 6. The TPD spectra of submonolayer, monolayer, and multilayer CH_2Cl_2 from FeO(111) for a variety of initial coverages (θ = 0.29, 0.49, 0.64, 0.79, 1.00, 1.26, 1.42, 1.76, 1.93, 2.13, 2.34, 2.83, and 3.01 ML).

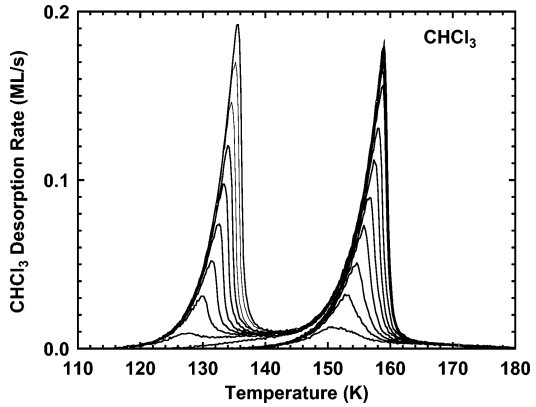

Figure 7. The TPD spectra for submonolayer, monolayer, and multilayer $CHCl_3$ from FeO(111) for a variety of initial coverages (θ = 0.17, 0.27, 0.37, 0.48, 0.59, 0.69, 080, 1.00, 1.14, 1.25, 1.34, 1.45, 1.58, 1.68, 1.80, 1.92, 2.02, and 2.14 ML).

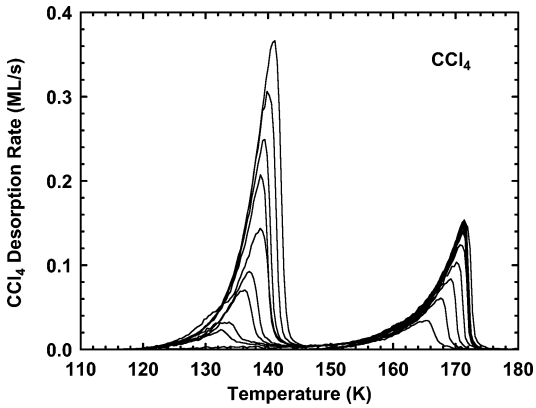

Figure 8. The TPD spectra for submonolayer, monolayer, and multilayer CCl_4 from FeO(111) for a variety of initial coverages (θ = 0.26, 0.43, 0.57, 0.76, 0.85, 1.00, 1.14, 1.27, 1.43, 1.60, 1.98, 2.18, 2.39, 2.78, and 3.15 ML).

to 40 K, respectively. The large temperature gap between the first layer and second layer desorption peaks demonstrates that, although CH_4 is weakly bound on the FeO(111) surface, the interaction between CH_4 and FeO is much stronger than that between the CH_4 adsorbates. The distinct leading edges of the zero-order desorption are observed for second, third, and fourth layers, indicating that the substrate stabilization effects are still discernible for at least 4 distinct layers.

Figures 5 through 8 show the TPD spectra of CH_3Cl, CH_2Cl_2, $CHCl_3$, and CCl_4 from the FeO(111) surface. As with that of methane, the spectra contain monolayer and multilayer desorption features. In general, the leading edges of the multilayer desorption features align on a common curve, indicating the expected zero-order desorption kinetics. However, most notably in the CH_3Cl TPD, the leading edges of some of the TPD spectra for the multilayer desorption feature cross. The crossing of the TPD spectra cannot be explained by simple desorption kinetics and is an indication of a phase change in the multilayer that occurs during the temperature ramp. This behavior has been observed previously in CH_3Cl,[35] CCl_4,[36] and H_2O[37] thin multilayer films.

The TPD line shapes of CH_3Cl (Figure 5) and CH_2Cl_2 (Figure 6) for submonolayer and monolayer coverages are similar to that of CH_4, (Figure 4) and show characteristics suggestive of zero- and first-order desorption kinetics. The $CHCl_3$ and CCl_4 TPD spectra have features (common leading edges and a sharp decrease in the desorption rate after the peak) characteristic of zero-order desorption. Zero-order desorption kinetics in the submonolayer coverage range have been observed previously for a number of adsorbates and substrates.[38−42] This type of desorption has been explained using thermodynamic equilibrium arguments invoking the coexistence of 2-dimensional (2D) islands with 2D gaslike phase of the adsorbate on the surface.[38−42] Following the phase rule, such a 2-phase coexistence leads to 2D vapor pressure that is independent of coverage and is defined only by the substrate temperature. Such behavior would lead to the zero-order desorption kinetics observed in the leading-edge region of the TPD spectra. Additionally, if the two-phase coexistence occurred only at lower temperatures and higher coverages, the first-order like line shape observed on the high-temperature falling edge of the CH_4, CH_3Cl, and CH_2Cl_2 TPD spectra may be indicative of the presence of a single 2D gaslike phase of these adsorbates.

The TPD spectra for CH_3Cl (Figure 5) are particularly interesting. This molecule possesses a large permanent dipole moment (1.89 D),[43] and one might expect the strong repulsive interactions between adsorbates to inhibit the formation of islands. Indeed, this type of behavior has been observed for CH_3Cl adsorbed on metals.[35,44] On metal surfaces, the $CHCl_3$ molecules adsorb with parallel electrical dipoles due to the formation of the image dipole in the substrate. The repulsive interactions between the dipoles of neighboring molecules result in a significant shift of the first-order TPD peaks to lower temperature with increasing initial coverage. FeO(111), in contrast to metal systems, is an electrical insulator with a low dielectric constant (ϵ = 14.2),[43] and no image dipole can be generated in the substrate. Consequently, the dipole moments (permanent and/or induced, see latter discussion) of the neighboring adsorbates are likely to be aligned in an antiparallel fashion rather than oriented in the same way. Similar arguments can be put forward in the case of $CHCl_3$ on FeO(111) shown in Figure 7.

D. Reactivity of O-Terminated FeO(111). To examine whether a certain fraction of the adsorbates dissociated, we monitored a number of possible mass fragments that would be expected on the basis of the molecules' cracking patterns. For example, the CH_2^+ and CH_3^+ fragments from CH_4, and the $CHCl^+$ and $CHCl_2^+$ fragments from $CHCl_3$ were recorded in addition to the mass of the parent molecules. The temperature profiles observed for all the fragments were always identical to those of the parent molecules. This suggests that the fragments do not arise from the dissociation of molecules on the surface but are the result of an ionization process in the quadrupole mass spectrometer. Further, no Fe- or other C-containing

fragments, e.g., $FeCl_2$ or CO, were observed in any of the TPD measurements. Such observations reveal that the adsorbates desorb from the FeO(111) surface intact without dissociation.

The fact that none of the adsorbates dissociate on the FeO-(111) surface is supported by the following evidence. The integrated area of the TPD spectra increases linearly with the exposure, demonstrating that no measurable consumption of the parent molecules occurred during the adsorption and desorption processes. Repeated experiments on the same FeO(111) film showed no change in the TPD line shape, indicating that no changes in the film composition or structure occurred due to prior exposures. Furthermore, all the TPD line shapes observed in this study show zero- or first-order characteristics, not the second-order characteristics commonly associated with dissociation and recombinative desorption processes. On the basis of the above observations, we conclude that the O-terminated FeO(111) surface is nonreactive with CH_4 and its chlorinated derivatives. This conclusion is consistent with previous studies[18−21] of water and ethylbenzene adsorption on FeO(111). In both cases, only molecular adsorption was observed. This is in sharp contrast with the dissociative adsorption that occurs on Fe_3O_4-(111) which possesses 1/4 monolayer of Fe on the surface.[18−21]

E. Desorption Kinetics. The TPD spectra were analyzed using the Polanyi−Wigner equation:

$$-\frac{d\theta}{dt} = \nu(\theta)\exp[-E(\theta)/RT]\theta^n \qquad (1)$$

where θ is the adsorbate coverage, n is the desorption order, t is time, $\nu(\theta)$ is the coverage dependent preexponential factor for desorption, $E(\theta)$ is the coverage-dependent desorption energy, R is the universal gas constant, and T is the temperature. Temperature and time are related by the heating rate, β, where $\beta = dT/dt$, and in our experiments was 1 K/s.

To obtain $E(\theta)$, we assume ν to be independent of θ. Since it is unclear from a simple inspection of the TPD spectra whether the desorption occurs via a zero- or first-order desorption process, we analyzed the data using both $n = 0$ and $n = 1$. With these assumptions, $E(\theta)$ can be calculated for each TPD spectrum as follows:

$$E(\theta) = -RT\ln\left(-\frac{\beta}{\nu}\frac{d\theta}{dT}\right) \quad \text{for } n = 0 \qquad (2)$$

and

$$E(\theta) = -RT\ln\left(-\frac{\beta}{\nu}\frac{d\theta}{\theta\, dT}\right) \quad \text{for } n = 1 \qquad (3)$$

In the analysis, ν is varied until the E vs θ curves obtained from TPD with different initial coverages retrace each other. This procedure was discussed in great detail in our previous studies[30] and therefore only the final $E(\theta)$ dependences are presented here.

As mentioned above, for CH_4, CH_3Cl, and CH_2Cl_2 we are unable to determine the order of desorption by simple inspection of the TPD spectra line shapes. Therefore, we performed the inversion of TPD spectra assuming both zero- and first-order kinetics for all of the molecules (including $CHCl_3$ and CCl_4) to obtain $E(\theta)$. The value of ν was the same for both $n = 0$ and $n = 1$ analysis. The values for ν were determined to be 1×10^{15} ML^{1-n} s^{-1} for CH_4, CH_3Cl, CH_2Cl_2, and $CHCl_3$, and 1×10^{12} ML^{1-n} s^{-1} for CCl_4. The error in the preexponential factor is estimated to be on the order of ± 1 order of magnitude, i.e., $1 \times 10^{15\pm1}$ and $1 \times 10^{12\pm1}$ ML^{1-n} s^{-1}. A factor of 10 change in the preexponential factor will result in an error of about $\pm 7\%$ in the determination of the desorption energy. The prefactors used in the analysis are summarized in Table 1.

TABLE 1: Monolayer Desorption Kinetic Parameters

n	desorption parameters	CH_4	CH_3Cl	CH_2Cl_2	CCl_3H	CCl_4
0	ν [ML/s]	10^{15}	10^{15}	10^{15}	10^{15}	10^{12}
	E_d [kJ/mol]	16.6	34.1	43.1	47.8	43.0
1	ν [s^{-1}]	10^{15}	10^{15}	10^{15}	10^{15}	10^{12}
	E_d [kJ/mol]	16.3	33.5	42.2	46.8	41.0

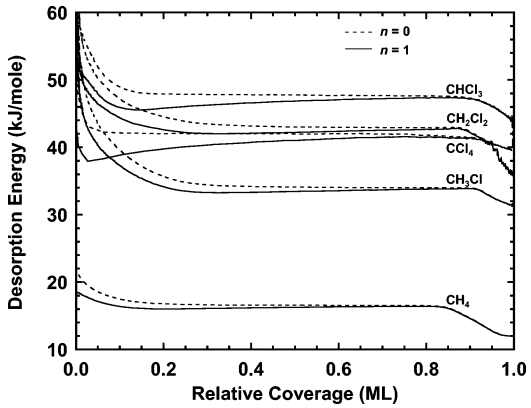

Figure 9. Desorption energies assuming a desorption order of $n = 0$ and $n = 1$, calculated by the inversion of Polanyi−Wigner equation. Dashed lines are for $n = 0$, and solid lines are for $n = 1$.

The large difference between the CCl_4 prefactor (10^{12}) and the other prefactors (10^{15}) is a bit puzzling. Within the framework of transition state theory the desorption prefactor, υ, is given by $(kT/h) \times (Q^*/Q)$ where k is Boltzmann's constant, T is temperature, h is Planck's constant, and Q and Q^* are the partition functions for the adsorbed and transition states, respectively.[45] At 170 K, kT/h has a value of $\sim 3.5 \times 10^{12}$ s^{-1}. Prefactors greater than $\sim 10^{13}$ suggest that the transition state is more gas phase-like than the tightly bound immobile adsorbate and as such has a larger partition function and higher entropy. Based on mass and moment of inertia considerations, the gas-phase partition function for the chlorinated methanes will be greatest for CCl_4. Hence, one would expect CCl_4 to have the largest desorption prefactor. Two effects could give rise to the small prefactor observed for CCl_4. First, the transition state may be much more constrained than that of the other molecules. Alternatively, the CCl_4 adsorbed state may be much more free molecule-like than the other molecules. The resolution of this puzzle will require a detailed knowledge of the potential energy surface and a full transition state theory calculation. For the purposes of the present paper, we find that a prefactor of 10^{12} for CCl_4 clearly gives the best fit to the TPD data and we use it in the energy analysis without further comment.

Figure 9 shows the $E(\theta)$ curves calculated in the manner outlined above for all the molecules studied. For simplicity, only the ~ 1 ML curve for each molecule is shown. The dashed lines are the $E(\theta)$ curves obtained assuming zero-order desorption ($n = 0$) and the solid lines are the $E(\theta)$ curves obtained assuming first-order desorption ($n = 1$). The results for the $n = 0$ and $n = 1$ analysis are nearly identical. For example, if we take the desorption energy at 0.5 ML, the difference between the values from $n = 0$ and $n = 1$ curves is only $\sim 2\%$ for all of the adsorbates. The activation energies at 0.5 ML calculated for $n = 0$ and $n = 1$ are listed in Table 1. The compound error in the determination of $E(\theta)$ results from the uncertainty of ν and n and is estimated to be $\sim 10\%$. These results demonstrate that

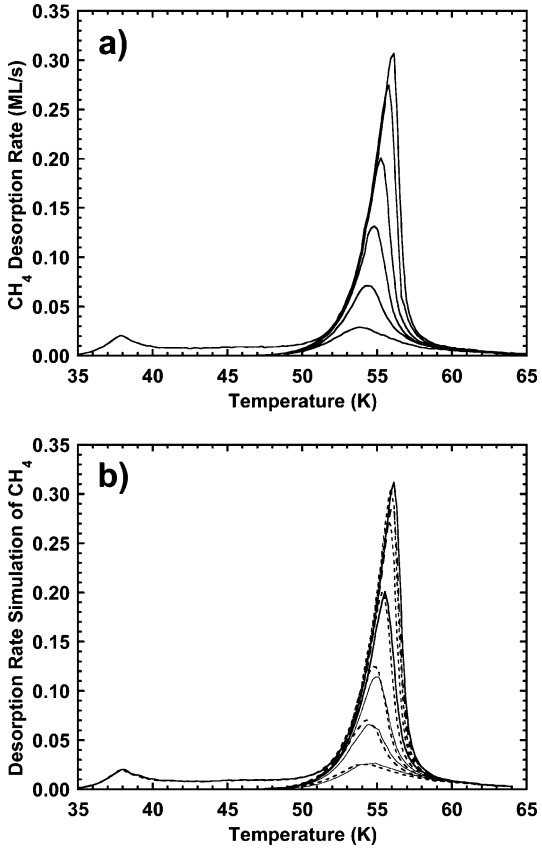

Figure 10. (a) A subset of the experimental CH_4 TPD spectra of monolayer and submonolayers coverages from Figure 4. (b) Simulated CH_4 TPD spectra assuming a desorption order of $n = 0$ (dashed lines) and $n = 1$ (solid lines).

the desorption energy is largely insensitive to the assumed desorption order at the terrace sites.

The analysis also reveals that the desorption energy coverage dependence can be categorized into three different coverage regions. At low coverages (below ~0.2 ML), the desorption energy increases sharply with decreasing coverage. This is due to the desorption from defect sites and defect influenced sites. Similar behavior was observed for adsorbates on MgO(100) in our previous studies.[30,46] For coverages between 0.2 ML and 0.85 ML, the desorption energy is nearly constant as the adsorbates desorb from ideal terrace sites. For coverages greater than 0.85 ML, the desorption energy decreases with increasing coverage. This decrease is related to the compression of adsorbed layer and repulsive interactions between the adsorbates.[30,46,47]

The accuracy of this analysis can be checked by using the extracted desorption parameters, ν and $E(\theta)$, to simulate the complete set of desorption spectra for CH_4 by numerical integration of the Polanyi−Wigner equation. As an example, we illustrate the process for CH_4. The $E(\theta)$ curve extracted from the CH_4 TPD of the saturated monolayer (shown in Figure 9) is used to simulate a set of desorption curves for different initial coverages. Figure 10a shows the experimental CH_4 TPD for $\theta \leq 1$ ML (a subset of the data in Figure 4). Figure 10b shows the simulated CH_4 desorption rate for $n = 0$ (dashed lines) and $n = 1$ (solid lines). Since the desorption energy is nearly the same for $n = 0$ and $n = 1$, the simulated desorption rates with $n = 0$ and $n = 1$ are very close to each other. There is also good agreement between the simulated and experimental results. The same level of agreement was obtained for all of the other molecules.

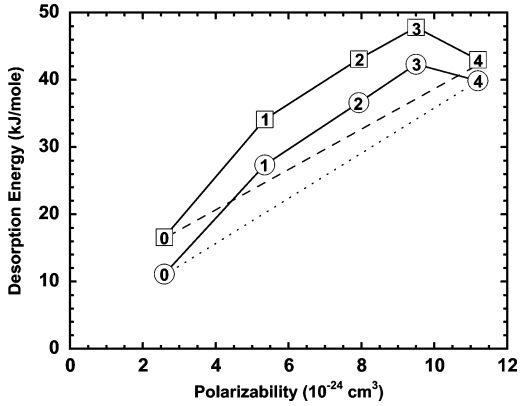

Figure 11. The monolayer and multilayer desorption energies plotted versus molecular polarizability of the molecules. The squares are the monolayer energies and circles are multilayer energies. The numbers within the symbols refer to the number of chlorine atoms in the molecules (e.g., 0 is CH_4, 1 is CH_3Cl, 2 is CH_2Cl_2, etc.). The dashed and dotted lines connect the desorption energies of CH_4 and CCl_4.

TABLE 2: Multilayer Desorption Kinetic Parameters

n	desorption parameters	CH_4	CH_3Cl	CH_2Cl_2	CCl_3H	CCl_4
0	ν [ML/s]	10^{15}	10^{15}	10^{15}	10^{15}	10^{14}
	E_d [kJ/mol]	11.1	27.3	36.6	42.3	39.9

The terrace site monolayer desorption energies obtained in the analysis generally increase with the number of chlorine atoms and hence the molecular mass (see Table 1). This indicates that the binding energy is primarily due to physisorption and as such, should be proportional to the molecular polarizability. Figure 11 shows the monolayer and multilayer desorption energies plotted versus the polarizability of the molecules.[43] The monolayer desorption energies are the terrace values ($\theta = 0.5$ ML) obtained from the $n = 0$ kinetic analysis listed in Table 1. The multilayer desorption energies are obtained from an analysis similar to that of the monolayer, assuming $n = 0$ for all molecules. Except for CCl_4, the same prefactors (1×10^{15} ML^{1-n} s^{-1}) used for the monolayer desorption data, also fit the multilayer desorption data. In the case of CCl_4, the best fits were obtained for ν equal to 1×10^{14} ML s^{-1} and 1×10^{12} ML^{1-n} s^{-1} for of the multilayer and monolayer desorption, respectively. The multilayer desorption kinetic parameters for all the molecules are listed in Table 2.

In Figure 11, the squares are the monolayer desorption energies and the circles are the multilayer desorption energies. The numbers within the symbols refer to the number of chlorine atoms in the molecules (e.g., 0 is CH_4, 1 is CH_3Cl, 2 is CH_2Cl_2, etc.). The solid lines connect the energies of the five molecules. The dashed and dotted lines connect the desorption energies of the CH_4 and CCl_4 monolayer and multilayers, respectively. The CH_4 and CCl_4 molecules have no permanent dipole moment, and as such, the desorption energy for these physisorbed molecules should be proportional to their corresponding polarizabilities.[46] Because the polarizability of these molecules increases approximately linearly with the number of chlorine atoms in the molecule, one might expect for the desorption energies from the monolayer and multilayers to increase linearly (i.e., lie on the dashed and dotted lines). However, this prediction does not account for the additional binding energy that results from the presence of a permanent dipole. The fact that the desorption energies of CH_3Cl, CH_2Cl_2, and $CHCl_3$ are higher than the corresponding value on the dashed lines is consistent with these molecules having a permanent dipole.[43] A quantitative determination of the fraction

of the binding energy due to the presence of a permanent dipole moment and the fraction due to the polarizability can only be done in combination with theoretical calculations.[35,48]

IV. Conclusions

The adsorption and desorption of methane (CH_4) and its chlorinated derivatives (CH_3Cl, CH_2Cl_2, $CHCl_3$, and CCl_4) on FeO(111) surface were studied using molecular beam scattering and temperature program desorption (TPD) techniques. High quality, epitaxial FeO(111) thin films were prepared using layer-by-layer deposition on Pt(111) surface[1] and characterized using low energy electron diffraction and N_2 physisorption.[30] The film defect densities determined from the N_2 physisorption were ~10% which is consistent with the defect density obtained with other high quality epitaxially grown oxides.[30] The TPD spectra of CH_4, CH_3Cl, CH_2Cl_2, $CHCl_3$, and CCl_4 show no evidence for dissociative adsorption or chemical reaction between the surface and the adsorbates. The inversion of the TPD spectra using zero- and first-order desorption yielded the preexponential factors and desorption energies for these adsorbates from FeO-(111). The increase of the binding energies with increasing polarizability of the molecules indicates that the adsorbate/surface interactions for all the molecules are primarily physisorption. We conclude that the O-terminated FeO(111) surface is inert with respect to the CH_4 and its chlorinated derivatives. These results provide a baseline comparison for future studies on the reactivity of other iron oxide phases, in particular those phases that have iron in the termination layer.

Acknowledgment. This work was sponsored by the U.S. Department of Energy Office of Basic Energy Sciences, Chemical Sciences Division. This work was performed at the W. R. Wiley Environmental Molecular Sciences Laboratory, a national scientific user facility sponsored by the Department of Energy's Office of Biological and Environmental Research and located at Pacific Northwest National Laboratory. Pacific Northwest National Laboratory is operated for the U.S. Department of Energy by Battelle under Contract No. DE-AC06-76RLO 1830.

References and Notes

(1) Weiss, W.; Ranke, W. *Prog. Surf. Sci.* **2002**, *70*, 1.
(2) Weiss, W.; Barbieri, A.; Vanhove, M. A.; Somorjai, G. A. *Phys. Rev. Lett.* **1993**, *71*, 1848.
(3) SchedelNiedrig, T.; Weiss, W.; Schlogl, R. *Phys. Rev. B* **1995**, *52*, 17449.
(4) Goodman, D. W. *Chem. Rev.* **1995**, *95*, 523.
(5) Freund, H. J.; Kuhlenbeck, H.; Staemmler, V. *Rep. Prog. Phys.* **1996**, *59*, 283.
(6) Campbell, C. T. *Surf. Sci. Rep.* **1997**, *27*, 1.
(7) Henry, C. R. *Surf. Sci. Rep.* **1998**, *31*, 235.
(8) Chambers, S. A. *Surf. Sci. Rep.* **2000**, *39*, 105.
(9) Weiss, W.; Ritter, M. *Phys. Rev. B* **1999**, *59*, 5201.
(10) Ritter, M.; Weiss, W. *Surf. Sci.* **1999**, *432*, 81.
(11) Wang, X. G.; Weiss, W.; Shaikhutdinov, S. K.; Ritter, M.; Petersen, M.; Wagner, F.; Schlogl, R.; Scheffler, M. *Phys. Rev. Lett.* **1998**, *81*, 1038.
(12) Galloway, H. C.; Sautet, P.; Salmeron, M. *Phys. Rev. B* **1996**, *54*, 11145.
(13) Ritter, M.; Ranke, W.; Weiss, W. *Phys. Rev. B* **1998**, *57*, 7240.
(14) Roddatis, V. V.; Su, D. S.; Kuhrs, C.; Ranke, W.; Schlogl, R. *Thin Solid Films* **2001**, *396*, 78.
(15) Ranke, W.; Ritter, M.; Weiss, W. *Phys. Rev. B* **1999**, *60*, 1527.
(16) Kim, Y. J.; Westphal, C.; Ynzunza, R. X.; Galloway, H. C.; Salmeron, M.; VanHove, M. A.; Fadley, C. S. *Phys. Rev. B* **1997**, *55*, 13448.
(17) Shaikhutdinov, S. K.; Meyer, R.; Lahav, D.; Baumer, M.; Kluner, T.; Freund, H. J. *Phys. Rev. Lett.* **2003**, *91*.
(18) Joseph, Y.; Ranke, W.; Weiss, W. *J. Phys. Chem. B* **2000**, *104*, 3224.
(19) Joseph, Y.; Kuhrs, C.; Ranke, W.; Ritter, M.; Weiss, W. *Chem. Phys. Lett.* **1999**, *314*, 195.
(20) Ranke, W.; Weiss, W. *Surf. Sci.* **1998**, *414*, 236.
(21) Joseph, Y.; Kuhrs, C.; Ranke, W.; Weiss, W. *Surf. Sci.* **1999**, *435*, 114.
(22) Kendelewicz, T.; Liu, P.; Doyle, C. S.; Brown, G. E.; Nelson, E. J.; Chambers, S. A. *Surf. Sci.* **2000**, *453*, 32.
(23) Adib, K.; Camillone, N.; Fitts, J. P.; Rim, K. T.; Flynn, G. W.; Joyce, S. A.; Osgood, R. M. *Surf. Sci.* **2002**, *497*, 127.
(24) Camillone, N.; Adib, K.; Fitts, J. P.; Rim, K. T.; Flynn, G. W.; Joyce, S. A.; Osgood, R. M. *Surf. Sci.* **2002**, *511*, 267.
(25) Adib, K.; Totir, G. G.; Fitts, J. P.; Rim, K. T.; Mueller, T.; Flynn, G. W.; Joyce, S. A.; Osgood, R. M. *Surf. Sci.* **2003**, *537*, 191.
(26) Adib, K.; Mullins, D. R.; Totir, G.; Camillone, N.; Fitts, J. P.; Rim, K. T.; Flynn, G. W.; Osgood, R. M. *Surf. Sci.* **2003**, *524*, 113.
(27) Smentkowski, V. S.; Ellison, M. D.; Yates, J. T. *Surf. Sci.* **1990**, *235*, 116.
(28) Smentkowski, V. S.; Cheng, C. C.; Yates, J. T. *Langmuir* **1990**, *6*, 147.
(29) Smentkowski, V. S.; Cheng, C. C.; Yates, J. T. *Surf. Sci.* **1989**, *215*, L279.
(30) Dohnálek, Z.; Kimmel, G. A.; Joyce, S. A.; Ayotte, P.; Smith, R. S.; Kay, B. D. *J. Phys. Chem. B* **2001**, *105*, 3747.
(31) Schlichting, H.; Menzel, D. *Rev. Sci. Instrum.* **1993**, *64*, 2013.
(32) King, D. A.; Wells, M. G. *Surf. Sci.* **1972**, *29*, 454.
(33) Dohnálek, Z.; Kimmel, G. A.; McCready, D. E.; Young, J. S.; Dohnalkova, A.; Smith, R. S.; Kay, B. D. *J. Phys. Chem. B* **2002**, *106*, 3526.
(34) Briquez, S.; Girardet, C.; Goniakowski, J.; Noguera, C. *J. Chem. Phys.* **1996**, *105*, 678.
(35) Maschhoff, B. L.; Ledema, M. J.; Kwini, M.; Cowin, J. P. *Surf. Sci.* **1996**, *359*, 253.
(36) Blanchard, J. L.; Roberts, J. T. *Langmuir* **1994**, *10*, 3303.
(37) Speedy, R. J.; Debenedetti, P. G.; Smith, R. S.; Huang, C.; Kay, B. D. *J. Chem. Phys.* **1996**, *105*, 240.
(38) Nagai, K.; Hirashima, A. *Appl. Surf. Sci.* **1988**, *33*−*34*, 335.
(39) Nagai, K.; Hirashima, A. *Surf. Sci.* **1987**, *187*, L616.
(40) Winkler, A.; Pozgainer, G.; Rendulic, K. D. *Surf. Sci.* **1991**, *251*, 886.
(41) Ruizsuarez, J. C.; Vargas, M. C.; Goodman, F. O.; Scoles, G. *Surf. Sci.* **1991**, *243*, 219.
(42) Daschbach, J. L.; Peden, B. M.; Smith, R. S.; Kay, B. D. *J. Chem. Phys.* **2004**, *120*, 1516.
(43) *CRC Handbook of Chemistry and Physics*, 80th ed.; Lide, D. R., Ed.; CRC Press: New York, 1999.
(44) Livneh, T.; Lilach, Y.; Asscher, M. *J. Chem. Phys.* **1999**, *111*, 11138.
(45) Masel, R. I. *Principles of Adsorption and Reaction on Solid Surfaces*; John Wiley & Sons: New York, 1996.
(46) Dohnálek, Z.; Smith, R. S.; Kay, B. D. *J. Phys. Chem. B* **2002**, *106*, 8360.
(47) Kimmel, G. A.; Persson, M.; Dohnálek, Z.; Kay, B. D. *J. Chem. Phys.* **2003**, *119*, 6776.
(48) Maschhoff, B. L.; Cowin, J. P. *J. Chem. Phys.* **1994**, *101*, 8138.